Particle Swarm Optimization-Based Hazardous Configuration Identification and Dynamic Analysis for Industrial Robots

Lina Zhang [1,2,3,4,*] and Aldrin D. Calderon [1,3]

[1] School of Mechanical, Manufacturing, and Energy Engineering, Mapua University, Manila, Philippines
[2] School of Mechatronic Engineering, Zheng Zhou Business University, Zhengzhou, China
[3] School of Graduate Studies, Mapúa University, Manila, Philippines
[4] Zhengzhou Intelligent Electromechanical Engineering Research Center, Zhengzhou, China
Email: 326188578@qq.com (L.Z.); adcalderon@mapua.edu.ph (A.D.C.)
*Corresponding author

***Abstract*—This paper presents a method for identifying the hazardous configuration of a KUKA KR3 R540 Six-Degree-of-Freedom (6-DOF) industrial robot. A kinematic model is first established using the standard Denavit-Hartenberg (D-H) method, and a multi-body dynamic model is subsequently constructed by incorporating the Newton-Euler formulation. To identify the pose that induces the maximum joint torque, a search strategy based on the Particle Swarm Optimization (PSO) algorithm is proposed, implemented through co-simulation between Adams and MATLAB. The optimization objective is defined as maximizing the sum of the absolute driving torques of joints J_2 to J_6, with the corresponding joint angles serving as decision variables. The PSO algorithm, driven by MATLAB, generates candidate poses, while Adams performs high-precision dynamic computations. This framework enables an automated search across the high-dimensional joint space to iteratively locate the global optimum. Simulation results demonstrate that the proposed method effectively identifies the global most hazardous configuration, corresponding to a fully extended manipulator pose with $J_2 \approx -90.81°$ and $J_3 \approx 82.57°$. The maximum total joint torque in this configuration is approximately 182.47 N·m. These results provide crucial load boundary conditions for structural strength verification and lightweight design, while also offering valuable insights for the selection of key components in structural optimization.**

***Keywords*—KUKA robot, dynamic analysis, hazardous configuration, Particle Swarm Optimization (PSO), Adams-MATLAB co-simulation**

I. Introduction

The widespread deployment of robots across industrial, service, and medical fields [1–3] has made dynamic modeling and the identification of hazardous configurations crucial for ensuring operational reliability. Industrial robots, serving as core components in intelligent manufacturing, often operate near workspace boundaries or singularities when executing large-scale tasks such as material handling and assembly. Under these extreme configurations, joint actuators are frequently subjected to peak torques that significantly exceed their rated values, thereby increasing the risks of structural fatigue, reducer failure, and even catastrophic machine failure [4, 5]. Consequently, quantifying the joint mechanical limits under extreme poses not only provides a quantitative basis for structural safety verification and lightweight design but is also essential for guaranteeing reliable performance throughout the robot's entire lifecycle [6].

Currently, scholars worldwide employ various methods to investigate the dynamics and stress of robots under extreme configurations. Experimental methods [7, 8] and numerical traversal algorithms [9] are widely used; however, these approaches typically involve substantial computational loads and low efficiency, making them difficult to adapt for real-time analysis under complex working conditions. In recent years, intelligent optimization algorithms have provided new ideas for solving such complex optimization problems [10]. Among them, the Particle Swarm Optimization (PSO) algorithm has been widely applied in robot path planning and parameter identification due to its few parameters, fast convergence, and strong global search capability [11–13]. Although PSO has demonstrated excellent performance in robot trajectory planning [14], parameter identification, and control [15, 16], and its accuracy in kinematic analysis has been proven superior to traditional methods [17], existing research predominantly focuses on trajectory optimization and motion performance [18]. Studies that integrate the PSO algorithm with high-fidelity dynamic simulation for hazardous configuration identification and joint limit load analysis remain insufficient. The Adams-PSO co-simulation framework proposed in this paper effectively combines the high-precision multi-body dynamics computation capability of Adams (MSC Software, USA) with the powerful flexibility of MATLAB in algorithm development. This elevates the optimization

Manuscript received September 4, 2025; revised October 14, 2025; accepted November 24, 2025; published January 23, 2025.

accuracy from the kinematic or control level to the multi-body dynamics level, enabling rapid evaluation of extreme working conditions during the early design stage and providing a new technical pathway for hazardous configuration research [19–21]. In terms of efficiency, the guided search of the PSO algorithm replaces the blind enumeration of traditional numerical traversal methods in high-dimensional space, thereby avoiding the exponential growth of computational cost with joint dimensionality and achieving a qualitative improvement in computational efficiency.

To address the aforementioned research gaps, this study employs the KUKA KR3 R540 Six-Degree-of-Freedom (6-DOF) industrial robot as a research platform to investigate hazardous configuration identification and dynamic analysis through a co-simulation framework. Initially, the Newton-Euler formulation is adopted to develop the dynamic model, establishing a direct mapping between joint space configurations and the corresponding driving torques. Subsequently, a search strategy based on the PSO algorithm is proposed, with the objective of maximizing the sum of absolute joint torques, to automatically identify the most hazardous posture across the entire joint space. Furthermore, an Adams-MATLAB co-simulation platform is constructed, wherein Adams provides high-fidelity dynamic validation of the PSO-derived results, ensuring computational accuracy. Ultimately, this work elucidates the joint load distribution of the KR3 R540 under extreme static loading conditions, thereby providing critical data support and a theoretical foundation for structural strength validation and lightweight design.

In contrast to traditional methods reliant on simplified models, the Adams-MATLAB co-simulation framework developed in this work enables automated global search with high fidelity. Its core advantage lies in bypassing the explicit simplification and derivation of complex dynamic equations. By directly integrating the global exploration capability of the PSO algorithm with the high-fidelity physical computation of Adams, optimization is performed directly on the complete multi-body model. This approach inherently avoids errors induced by model simplification, thereby yielding more reliable identification of hazardous configurations and limit loads.

II. Theoretical Basis and Methodology

A. Foundation of Robot Dynamic Modeling

Robot dynamic modeling serves as the theoretical foundation for identifying hazardous configurations, with the objective of establishing the mapping between joint angles q and the required joint driving torques τ. Among the available modeling methodologies—including the Lagrangian formulation, Newton-Euler method, Gauss's principle, Kane's equations, and screw-dual number theory—the Lagrangian and Newton-Euler approaches are the most widely adopted [22]. The Lagrangian method, based on energy analysis, offers a concise formulation but suffers from high computational complexity, making it less suitable for rapid computation in multi-DOF robotic systems [23]. In contrast, the Newton-Euler method employs a recursive link-by-link derivation, resulting in significantly higher computational efficiency and rendering it particularly suitable for real-time dynamic analysis [24]. Since this study focuses on a 6-DOF robot under the most severe static loading condition in a gravitational field, and the dynamic model must be evaluated repeatedly during PSO iterations, the Newton-Euler method is selected for its computational advantage. The dynamic model is constructed based on the robot's geometric parameters and joint coordinate systems, with the D-H parameters listed in Table I.

TABLE I. D-H Parameter Table

Link i	θ_i (°)	d_i (mm)	a_i (mm)	α_i (°)	Joint Range (°)
1	θ_1	345	20	−90	±170
2	θ_2	0	260	0	−170/50
3	θ_3	0	20	−90	−110/155
4	θ_4	260	0	90	±175
5	θ_5	0	0	−90	±120
6	θ_6	75	0	0	±350

The general dynamic equation for an n-DOF serial industrial robot can be described by Eq. (1):

$$\tau(q,\dot{q},\ddot{q}) = M(q)\ddot{q}+C(q,\dot{q})\dot{q}+g(q)+J^T(q)F_{\text{ext}} \quad (1)$$

where:
$\tau=[\tau_1,\tau_2,\ldots,\tau_n]^T$ is the joint driving torque vector;
$M(q)$ is the joint-space inertia matrix;
$C(q,\dot{q})\dot{q}$ represents the Coriolis and centrifugal forces;
$g(q)$ denotes the gravitational torque;
$J(q)$ is the geometric Jacobian of the end-effector;
F_{ext} is the external wrench applied at the end-effector.

In applications such as spot welding, the holding phase in material handling, or when determining limit loads for design verification, robot velocity and acceleration are zero or negligible. Under these conditions, inertial and Coriolis forces can be disregarded. Therefore, this study focuses on the most severe static loading condition within a gravitational field, where the dynamic model considers only the gravitational and external load terms, while joint velocities and accelerations are set to zero, i.e., $\dot{q} = 0$ and $\ddot{q} = 0$, then the dynamic equation simplifies to Eq. (2):

$$\tau(q) = g(q)+J^T(q)F_{\text{ext}} \quad (2)$$

where:
$g(q)$ is determined by the mass and center-of-mass position of each link;
$J^T(q)F_{\text{ext}}$ represents the joint torque load resulting from the projection of the external end-effector force through the Jacobian matrix.

Consequently, for the identification of static hazardous configurations, each joint angle vector q maps to a unique set of joint torques. The PSO algorithm is employed to search the high-dimensional joint space, enabling the identification of the specific configuration that maximizes the total load on the robotic manipulator.

B. Algorithm and Design

The PSO algorithm is a population-based global optimization technique inspired by the collective social behavior of bird flocking or fish schooling, originally introduced by Kennedy and Eberhart [25]. This metaheuristic algorithm models the cooperative search process of a swarm of particles, each of which iteratively updates its position within the search space to progressively approach the optimum. In comparison with conventional optimization approaches, PSO is characterized by its simplicity of implementation, minimal parameter tuning, and robust global exploration capability. Throughout the iterative process, each particle dynamically adjusts its velocity and position according to its own historical best solution (personal best, pbest) and the swarm's overall best solution (global best, gbest), facilitating coordinated evolution toward promising regions of the search space [26]. Through successive generations, the swarm collectively converges to the optimal or a near-optimal solution, with the overall procedure summarized in Fig. 1.

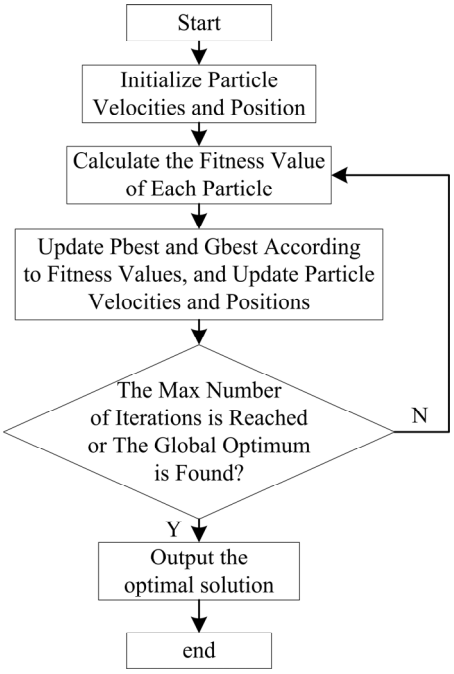

Fig. 1. PSO calculation diagram.

In this study, the PSO algorithm is employed to identify the most hazardous configuration of the KUKA KR3 R540 robot within a gravitational field. The optimization objective for hazardous configuration identification is to locate the pose that induces the most severe overall load on the manipulator. To prioritize the analysis of hazardous loads on major working joints, Joint 1—serving as the base rotation axis—was excluded from the optimization variables due to its negligible influence on the gravitational moment. The optimization variables were ultimately defined as the angles of Joints 2 to 6 (q_1, q_2, q_3, q_4, q_5), resulting in an optimization dimension of $d = 5$. The fitness function for the PSO is defined as the sum of the absolute driving torques of Joints 2 through 6, which is to be maximized. The specific design is outlined as follows:

(1) Optimization variables: The particle dimension is set to $d = 5$, corresponding to the robot's five joint angles forming the vector $q = [q_1, q_2, q_3, q_4, q_5]^T$, where q_1 to q_5 represent the angular positions of Joints 2 through 6, respectively.

(2) Constraints: (1) Joint angle limits: $q_i^{\min} \leqq q_i \leqq q_i^{\max}$, for $I = 1, 2, \ldots, 5$, where the bounds are defined by the manufacturer-specified operating ranges; (2) Workspace and safety constraints: By restricting all joint angles to their official motion ranges and ensuring sufficient clearance between the end-effector and both the workpiece and robot base, workspace and collision-avoidance constraints are inherently satisfied.

(3) Objective Function: The sum of the absolute joint torques is adopted as the objective function, expressed in Eq. (3), to comprehensively evaluate the global load severity of the robot under different configurations:

$$f_{\text{sum}}(q) = \sum_{i=1}^{5} |\tau_i(q)| \tag{3}$$

where:

$\tau_i(q)$ denotes the driving torque required by the i-th joint at configuration q;

$|\tau_i(q)|$ is the absolute value of the joint torque, which is used to measure the load magnitude regardless of its direction;

$f_{\text{sum}}(q)$ is the overall objective function value, reflecting the cumulative load level of the considered joints at configuration q.

This metric captures the combined torque demand across all joints at a given configuration, providing a comprehensive measure of the robot's overall load condition. Unlike approaches that consider only the maximum individual joint torque, this summed-value formulation accounts for potential loading across all actuated joints, thereby offering a more complete characterization of globally hazardous configurations. Consequently, the summation of joint torque magnitudes is selected as the optimization objective, with its maximization serving as the convergence criterion for the PSO iterations.

(4) Convergence criterion: The maximum iteration count is set to generation (ger) = 50. The convergence criterion is defined as follows: if the improvement in the global best fitness value remains below 1×10^{-6} N·m for 20 consecutive generations, the algorithm is considered to have converged and terminates early.

With the above optimization setup, the PSO algorithm efficiently identifies near-optimal hazardous configurations—where the joint loads approach their limits—within a constrained iteration budget. The resulting optimal pose is subsequently validated through dynamic simulation in the Adams environment.

C. Adams-MATLAB Co-Simulation Principle

Adams is an industry-standard multi-body dynamics software capable of high-fidelity simulation of mechanical systems under gravitational, inertial, and external loads. MATLAB provides a powerful environment for numerical computing and optimization algorithm implementation, particularly suitable for executing PSO [27, 28]. The Adams-MATLAB co-simulation framework establishes a closed-loop analysis system: MATLAB serves as the optimization host, executing the PSO algorithm and generating decision variables (joint angles), while Adams functions as the high-precision mechanical solver, computing the corresponding joint torques and returning results to guide the optimization. The complete co-simulation workflow is illustrated in Fig. 2. This methodology has been successfully demonstrated in complex transmission systems, confirming the viability of integrating dynamic modeling with optimization techniques [29, 30].

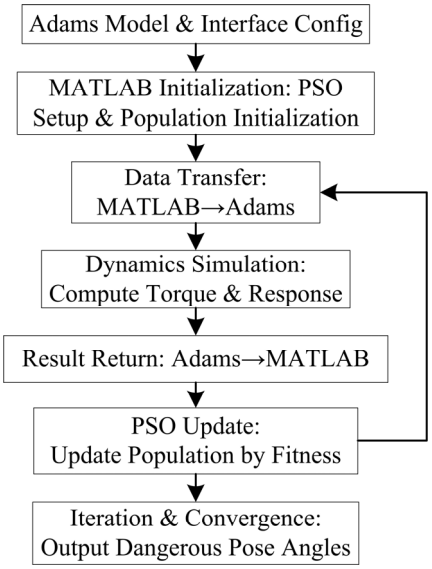

Fig. 2. Flowchart of the Adams-MATLAB co-simulation process.

III. Simulation Process and Results Analysis

A. Simulation Process and Parameter Settings

1) Establishment of the Adams multi-body dynamics model

Due to limitations in robot modeling within Adams, the three-dimensional model of the robot was created in SolidWorks and imported into Adams in Parasolid format. To enhance simulation fidelity, non-structural components with negligible effects on the results were removed prior to simulation, thereby highlighting the core mechanical structure and reducing computational cost [31]. To improve the accuracy of dynamic analysis [32], actual mass and center-of-mass parameters were assigned to each component and the end-effector, as summarized in Table II. 6 revolute joints were created between adjacent links, with their axes consistent with the definitions in the D-H parameter table. The resulting assembly is shown in Fig. 3. A rotational motion driver was defined for each joint, with its displacement function specified as VARVAL (.model_1.INT_AG*i*) (where i = 1–6), providing an interface for MATLAB control. A measurement of type Motion Force → Torque about Z was created for each driver to output the joint driving torque. Gravity was set to -9.81 m/s^2 along the Y-axis of the global coordinate system to simulate the actual gravitational environment.

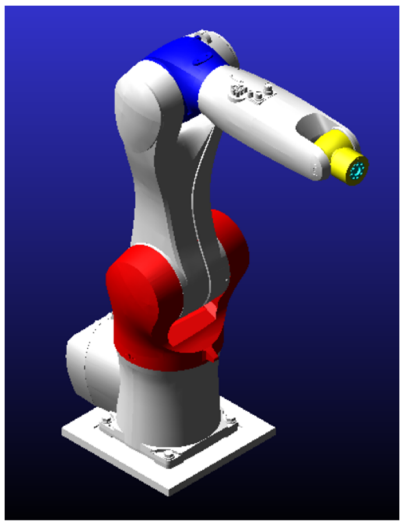

Fig. 3. Simplified 3D model of the robot.

TABLE II. Total Mass and Center of Gravity of Robot Components

Link *i*	m_i (kg)	r_{xi} (mm)	r_{yi} (mm)	r_{zi} (mm)
1	8.65	44.48	−0.05	110.09
2	5.09	7.97	2.01	332.72
3	7.49	18.03	3.98	603.48
4	2.36	41.08	0.02	865.49
5	2.46	279.60	−0.07	890.30
6	0.45	461.61	1.89	889.97
End of Arm Tooling (EOAT)	2.00	517.48	0.00	890.04

2) Co-simulation principle and configuration

Within the co-simulation framework of this study, dynamic computations are handled by Adams, which utilizes the Generalized STIFF (GSTIFF) integrator for solution. The MATLAB/Simulink environment acts as the master controller, executing the PSO algorithm, sending joint angle commands to Adams, and simultaneously receiving the resulting joint torque data from Adams. Data exchange between the two platforms is performed via fixed-step communication.

3) Robot parameters and static working condition constraints

The kinematic D-H parameters and joint motion ranges of the robot in this study are listed in Table I. The simulation focuses on static conditions, neglecting inertial and Coriolis forces during motion and considering only gravitational loads. A 2 kg End of Arm Tooling (EOAT) is mounted on the robot's end flange as a simulation payload, with no additional external operational forces applied. The search space for each joint angle is constrained by its official motion range.

4) PSO optimization algorithm parameter settings

The PSO algorithm is employed to efficiently search for the most hazardous configuration across the entire joint space. Based on the kinematic characteristics of serial robots, hazardous configurations typically occur at mechanically extreme positions where the manipulator is fully extended or retracted [33, 34]. To effectively identify static hazardous configurations, this study focuses the optimization variables on the joints most sensitive to gravitational loading. Preliminary analysis indicates that Joints 2 and 3—driving the upper arm and forearm, respectively—are the dominant factors influencing the overall gravitational moment, and are therefore treated as the core of the analysis. Wrist Joints 4–6 are also included to account for their potential coupling effects. Using the robot configuration shown in Fig. 3 as the initial zero position, with counterclockwise rotation defined as positive and clockwise as negative for each link, the optimization ranges for each joint variable are set according to official data, as listed in Table III.

TABLE III. THE OPTIMIZATION RANGE OF EACH JOINT VARIABLE

Joint No.	J_2	J_3	J_4	J_5	J_6
Motion Range (°)	−140/8 0	−155/11 0	±200	±150	±200

The population size N is set to 20, with a maximum iteration count of 50. The algorithm parameters are configured as follows: inertia weight w = 0.8, individual learning factor c_1 = 0.7, and social learning factor c_2 = 0.9. These parameter values, established based on typical empirical values for robotic optimization problems [26] and preliminary testing, strike an effective balance between exploration and exploitation. The optimization objective is to maximize the sum of absolute driving torques for robot Joints 2 to 6, expressed as $\max f_{\text{sum}}(q) = \sum_{i=1}^{5} |\tau_i(q)| (i = 1, 2, \ldots, 5)$.

5) Co-simulation interface configuration

Adams offers two primary co-simulation approaches: the script interface mode and the Simulink interface mode [35]. This work employs the Adams-Simulink co-simulation scheme, wherein the robot dynamics model—with explicitly defined input (joint angles) and output (joint torques) variables—is exported as a Simulink subsystem block (adams_sub) via the Adams/Controls module. The complete simulation architecture is implemented in Simulink, with the resulting co-simulation block diagram presented in Fig. 4. In this setup, the "simout → To Workspace" block serves to record and export the joint torque time-series data obtained from Adams simulation to the MATLAB workspace. The PSO algorithm then reads these data to compute the objective function value for the current configuration, thereby closing the optimization loop.

To ensure efficient and accurate computation of static torques in the co-simulation, the Simulink parameters are configured as follows: the simulation time is set to [0, 1] seconds. To achieve stable and synchronized data exchange with the Adams model, the co-simulation communication is configured with a fixed step size, employing a fixed-step solver. This configuration ensures reliable dynamic computation by Adams at each communication step. Accurate static torque results are obtained by reading the stabilized torque data at the final simulation time. During co-simulation, a MATLAB script drives the PSO algorithm to generate joint angle commands and invokes the Simulink model to transmit these commands to the subsystem. Adams receives the angle values in the background, performs dynamic computation, and returns the resulting joint torques to the MATLAB workspace [36]. This establishes an automated closed-loop optimization cycle of "MATLAB generates parameters → Adams performs precise computation → returned results guide optimization", thereby achieving automated identification of hazardous configurations.

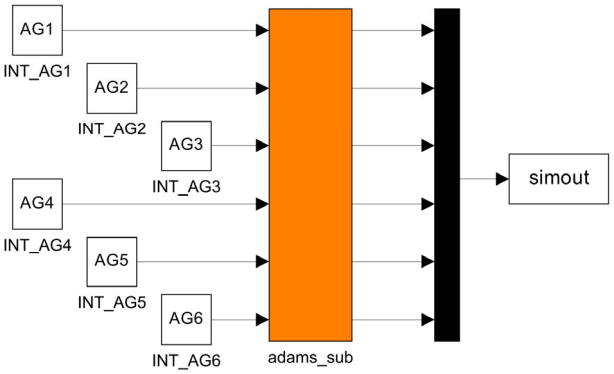

Fig. 4. Adams and Simulink co-simulation block diagram.

B. Optimization Results and Analysis

To validate the effectiveness of the proposed method, ten co-simulation optimizations were conducted using the parameters specified in the previous section. The evolution curves of the total torque, individual joint angles, and respective joint torques during the PSO process, obtained from the simulations, are presented in Figs. 5–7.

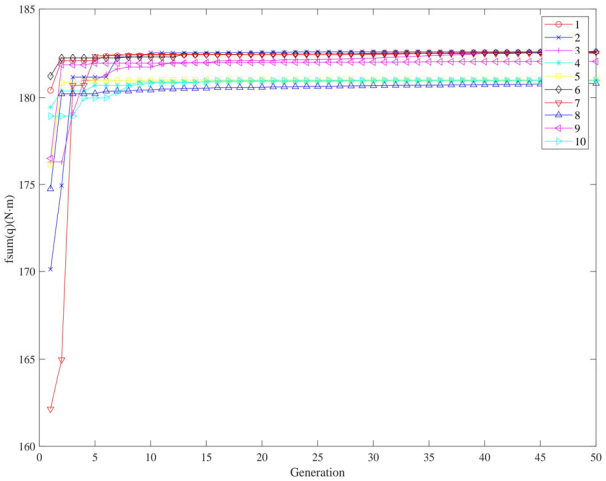

Fig. 5. Curve of total torque vs. iteration number.

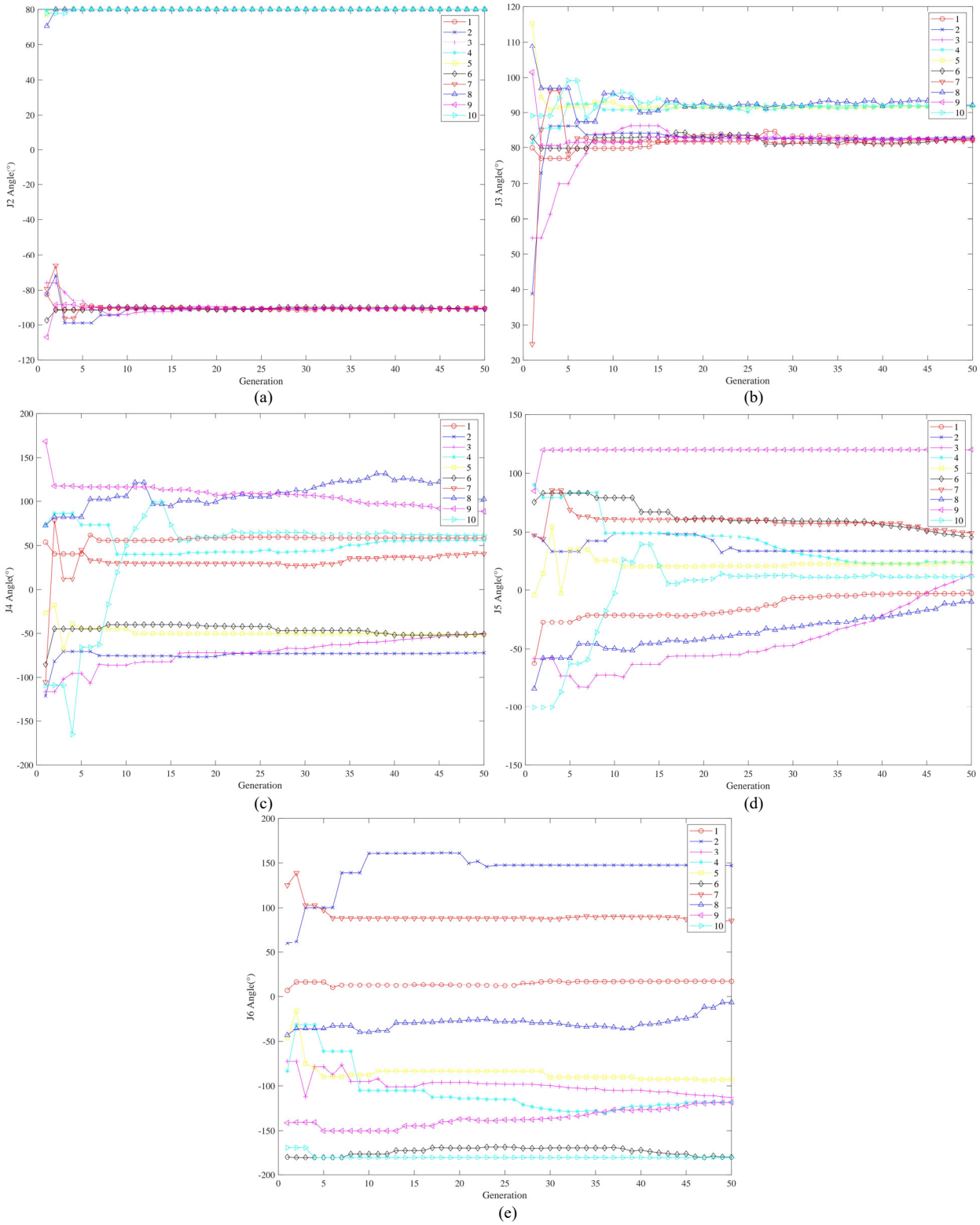

Fig. 6. Curves of each joint angle vs. iteration number. (a) J_2 angle vs. iteration number; (b) J_3 angle vs. iteration number; (c) J_4 angle vs. iteration number; (d) J_5 angle vs. iteration number; (e) J_6 angle vs. iteration number.

1) Algorithm convergence analysis

As shown in Fig. 5, the fitness values (total torque) from ten independent PSO runs demonstrate rapid growth with increasing iterations. The optimization process enters a rapid improvement phase around the 5th generation and collectively stabilizes after the 11th generation. Subsequently, all total torque values fluctuate minimally around the mean of 182 N·m, with a standard deviation of 0.82 N·m across the ten runs, indicating stable convergence to the global optimum. This convergence behavior confirms that the PSO parameters are appropriately configured and the optimization strategy exhibits high search efficiency and robustness.

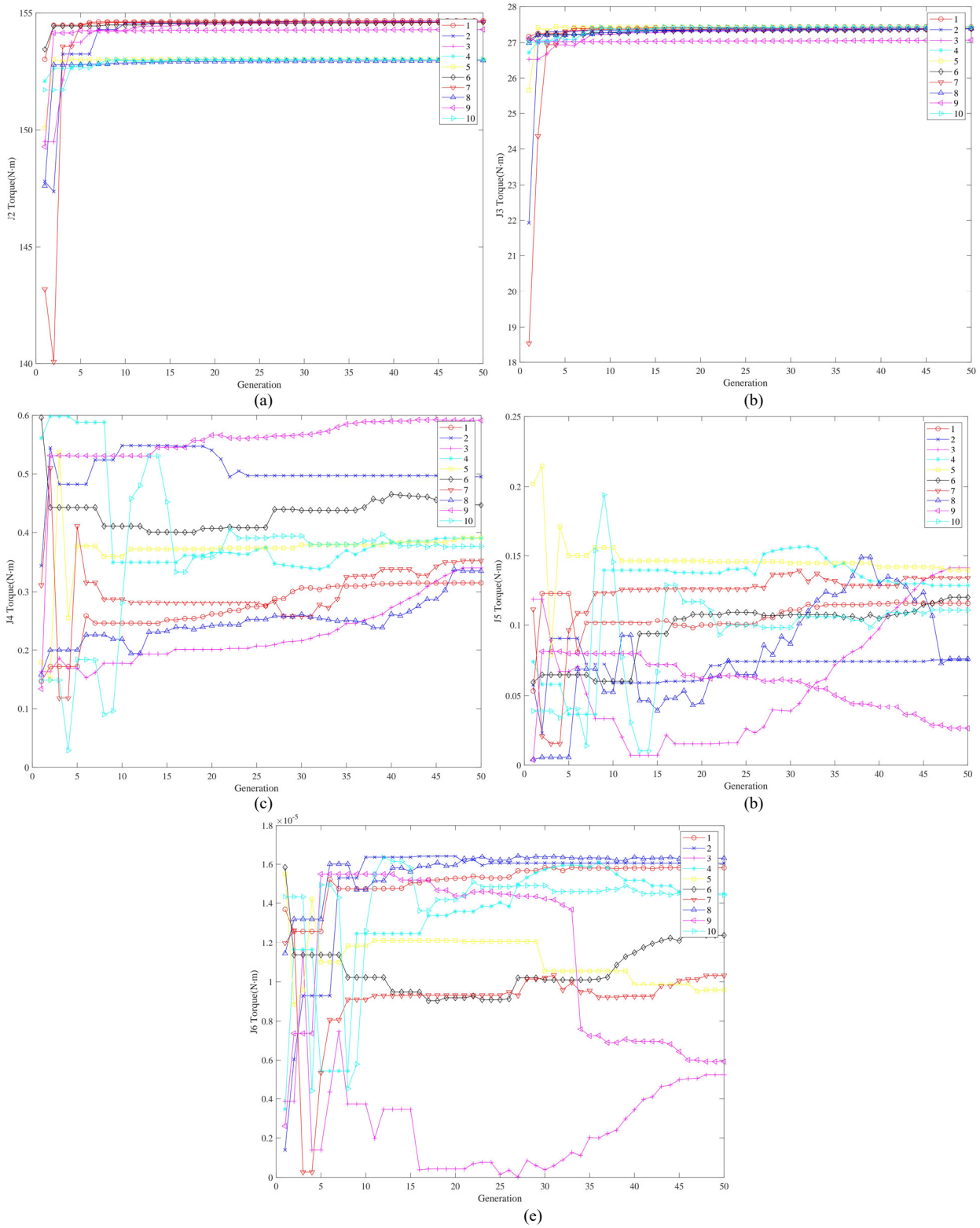

Fig. 7. Curves of each joint torque vs. iteration number. (a) J_2 torque vs. iteration number; (b) J_3 torque vs. iteration number; (c) J_4 torque vs. iteration number; (b) J_5 torque vs. iteration number; (e) J_6 torque vs. iteration number.

2) Analysis of joint angle optimization process

Analysis of the joint angle convergence curves in Fig. 6 reveals the following:

(1) Joints 2 and 3: The optimization processes of Joints 2 and 3 in Fig. 6(a) and (b) demonstrate core characteristics of the robot's static hazardous configurations. Unlike the random search patterns observed in the wrist joints, the angles of J_2 and J_3 exhibit clear, rapid convergence trends across all 10 runs, yet their final results distinctly separate into two clusters:

- Forward-extended posture: In the majority of runs, J_2 converges to approximately −91°, and J_3 to

approximately 82°. This configuration corresponds to the manipulator fully extending forward and downward, positioning the robot's center of gravity at its farthest limit from the base.

- Backward-leaning posture: In some runs, J_2 converges to approximately 80°, and J_3 to approximately 91°. In this configuration, the manipulator extends backward and downward.

The PSO algorithm's ability to comprehensively capture both configurations demonstrates its strong global exploration capability. Although the total torques are very similar between these postures, their potential failure risks differ significantly. In industrial robots, Joint 2 being closer to the base, is typically designed to be the strongest with a higher rated torque. In contrast, Joint 3 of the forearm, as a downstream element in the kinematic chain, is structurally more vulnerable and typically has a lower rated torque. Therefore, analysis of the forward-extended posture holds greater engineering significance for safety: this posture loads the relatively weaker Joint 3 near its mechanical limit, creating the most hazardous "weakest link" in the system [32]. The results corresponding to the forward-extended posture from the ten runs are summarized in Table IV. This posture shows a mean total torque of 182.47 N·m, with mean joint angles of −90.81° for J_2 and 82.57° for J_3. The corresponding standard deviations are 0.22 N·m, 0.13°, and 0.31°, respectively. These results confirm that the adopted PSO parameters provide excellent robustness, enabling the algorithm to stably and repeatedly locate the global most hazardous configuration.

(2) Joints 4, 5 and 6: In sharp contrast to J_2 and J_3, the optimization processes of the wrist joints (J_4, J_5, J_6) in Fig. 6(c)–(e) exhibit random search characteristics without consistent patterns. Although some angles tend to stabilize towards the end of iterations, their final values demonstrate high discreteness across the 10 independent runs, as indicated in Table IV. This confirms that the posture variations of the wrist joints have a negligible influence on the total gravitational moment of the manipulator. During the search, the PSO algorithm recognized that adjusting these joints could not significantly improve the value of the objective function (total torque), and therefore did not treat them as key decision variables. This finding strongly supports the adoption of a dimensionality-reduction optimization strategy focusing solely on Joints 2 and 3 in subsequent research or engineering applications, which would substantially improve computational efficiency.

TABLE IV. COMPUTATION RESULTS FOR THE FORWARD-EXTENDED POSTURE

Variable	Run 1	Run 2	Run 3	Run 4	Run 5	Run 6
f_{sum} (q) (N·m)	182.54	182.59	182.61	182.57	182.51	181.99
J_2(°)	−90.63	−90.89	−90.87	−91.02	−90.69	−90.78
J_3(°)	82.14	83.15	82.47	82.71	82.38	82.59
J_4(°)	58.26	−71.49	−50.39	−50.87	40.77	88.77
J_5(°)	−2.72	32.57	13.61	45.49	49.14	120.00
J_6(°)	17.35	147.04	−112.76	−179.62	85.60	−117.96

Based on the comprehensive analysis above, this study selects the "forward-extended posture"—which imposes more severe loading on Joint 3—from the two hazardous configurations identified by PSO as the limit condition with the greatest engineering safety significance. Accordingly, the static hazardous configuration of the robot is determined as $J_2 \approx -90.81°$ and $J_3 \approx 82.57°$. This result deviates from the theoretically expected posture ($J_2 = -90°$, $J_3 = 90°$) based on the assumption of uniform mass distribution [37]. The discrepancy primarily stems from the asymmetric mass distribution and center-of-mass offsets among the robot links, demonstrating that the maximum joint load does not simply occur at the fully horizontal arm geometry but is determined by the actual physical attributes of the structure.

3) Analysis of the joint torque optimization process

As illustrated in Fig. 7, the evolutionary trajectories of individual joint torques exhibit strong coupling with their corresponding angle optimization processes, leading to the following conclusions:

(1) Joints 2 and 3: Their torque values are significantly higher than those of other joints, representing the dominant contributors to the overall load. The variation trends of these torques are highly consistent with the total torque curve in Fig. 5, directly determining the direction of the optimization objective. The final mean converged torque values are approximately 153.96 N·m for Joint 2 and 27.38 N·m for Joint 3, summing to 181.34 N·m, which accounts for 99.38% of the total torque.

(2) Joints 4, 5 and 6: In contrast to the random distribution of their angles, their output torques remain consistently at minimal levels across all runs. This indicates that the posture of the wrist joints has a negligible influence on the global static load. During optimization, these joints do not function as critical decision variables; their angle values merely passively adapt to the macro configuration determined by the primary arm joints (Joints 2 and 3), and the randomness in their own postures does not significantly affect the total torque.

4) Sensitivity analysis of wrist joints

To evaluate the influence of wrist joints on the global static load, supplementary validation simulations were conducted based on the identified optimal configuration of the dominant joints. Specifically, with Joints 2 and 3 fixed in the forward-extended hazardous posture, random sampling was performed across the full motion range of

the wrist joints. The resulting mean joint torques and their standard deviations are summarized in Table V. The computational results demonstrate that despite substantial variations in wrist joint angles, the standard deviations of the corresponding joint torques do not exceed 0.1670 N·m, while the standard deviation of the total torque is merely 0.36 N·m—representing a fluctuation of less than 0.2% relative to its mean value. These results quantitatively confirm that posture variations of the wrist joints have a negligible effect on the identification of global hazardous configurations. This finding not only validates the initial decision to focus the optimization variables on the primary joints but also provides a solid mathematical foundation for proposing a more efficient dimensionality-reduction optimization strategy.

TABLE V. JOINT TORQUES AND STANDARD DEVIATIONS FROM WRIST JOINT SENSITIVITY ANALYSIS

Joint No.	$f_{sum}(q)$	J_2	J_3	J_4	J_5	J_6
Mean Torque (N·m)	181.92	154.39	27.20	0.25	0.08	0.00
Standard Deviations (N·m)	0.36	0.16	0.16	0.17	0.06	0.00

In summary, the static hazardous configuration of the KUKA KR3 R540 robot is predominantly governed by the postures of Joints 2 and 3, while the influence of Joints 4, 5, and 6 is negligible. The identified critical posture corresponds to the forward-fully-extended state of the manipulator, where the combined joint torque reaches its maximum with a mean value of 182.47 N·m.

C. *Verification of Co-Simulation Results and Error Analysis*

To validate the reliability of the hazardous configuration and maximum torque results obtained from the aforementioned PSO optimization, this section conducts an independent static analysis within the Adams model using the optimized maximum torque and its corresponding joint angles, followed by comparative results and error analysis.

1) *Hazardous configuration visualization*

The optimal joint angle combination identified by the PSO algorithm is applied as input to the Adams model, with the resulting static hazardous configuration presented in Fig. 8. The visualization clearly shows the robotic arm in a fully extended configuration with the upper arm and forearm reaching their maximum extension, positioning the center of gravity at its farthest point from the base. This geometric representation provides initial validation of the optimization results and aligns perfectly with the conclusions drawn from the torque and angle evolution analysis in Section III.B, confirming that the hazardous configuration is dominated by Joints 2 and 3 and corresponds to the fully extended arm posture.

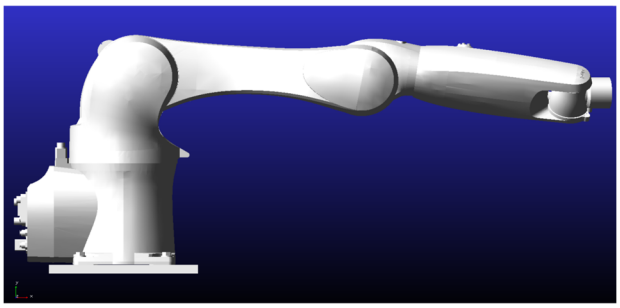

Fig. 8. Schematic diagram of the robot's hazardous configuration based on Adams.

Fig. 9 presents the transient driving torques of all joints computed by the Adams solver under this hazardous configuration. All joint torques rapidly stabilize within a very short duration, confirming that the robot reaches static equilibrium. The Adams results clearly demonstrate that the torques produced by the wrist joints (J_4–J_6) are negligible in the final posture, thereby corroborating from a mechanical perspective the conclusion presented in Section III.B.

2) *Results comparison and error analysis*

The steady-state values extracted from the curves in Fig. 9 serve as precise reference results from Adams for comparison with the PSO outcomes. A detailed comparison between the PSO-optimized results and the direct computational results from the high-fidelity Adams dynamic model is presented in Table VI.

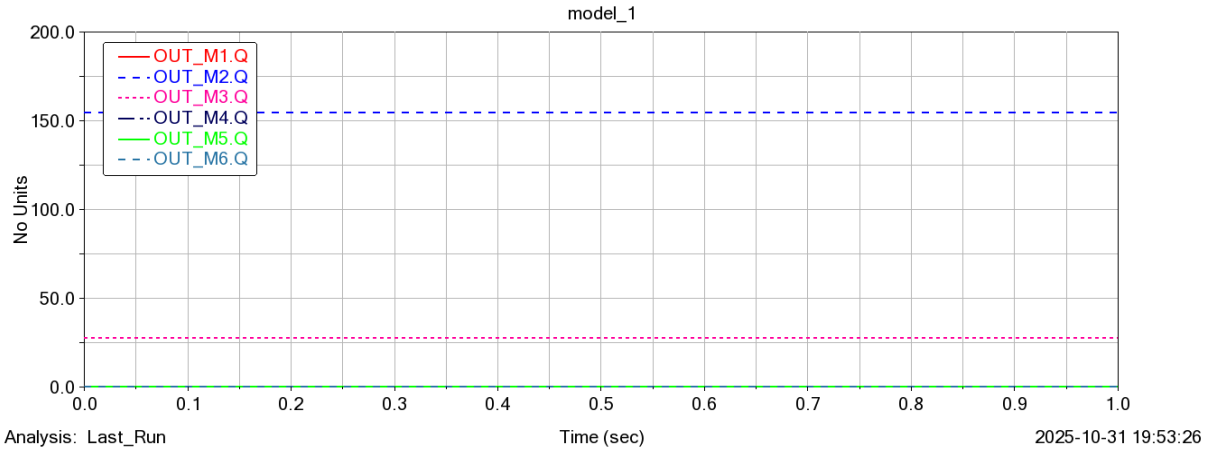

Fig. 9. Joint torque curves from Adams post-processing.

TABLE VI. COMPARISON OF RESULTS BETWEEN MATLAB-PSO AND ADAMS

Joint	MATLAB-PSO Torque (N·m)	Adams Torque (N·m)	Absolute Error (N·m)	Relative Error (%)
J_2	154.6765	154.6754	0.0011	0.0007
J_3	27.4399	27.4389	0.001	0.0036
J_4	0.3396	0.3535	−0.0139	−4.0931
J_5	0.1416	0.1470	−0.0054	−3.8136
J_6	0	0	0	0.0000
Total	182.5976	182.4678	0.1298	0.0711

Based on the data presented in Table VI, the following conclusions can be drawn:

(1) High Consistency: The maximum absolute torque error for the primary load-bearing joints (J_2, J_3) is merely 0.0011 N·m, with a maximum relative error of only 0.0036%. The total torque exhibits an absolute error of 0.1298 N·m and a relative error of 0.0711%, all falling within acceptable engineering tolerances. These results confirm that the PSO algorithm successfully located the true global optimum and demonstrate the reliability of the Adams-MATLAB co-simulation strategy.

(2) Error Source Analysis: The minor observed discrepancies can be attributed to the following factors:

- Numerical precision and interface transmission: Rounding errors inherent in the data exchange between MATLAB and Adams during co-simulation;
- Model fidelity: Subtle differences in parameter implementation between the simplified dynamics model used in PSO iterations and the high-fidelity Adams verification model;
- Solver configuration: Discrepancies between the simplified static solution employed in the PSO loop and the high-precision solver settings used in Adams post-processing analysis.

D. Result Discussion and Outlook

Through precise identification of hazardous configurations and dynamic analysis, this study provides critical input loads and universal design guidelines for the lightweight design of 6-DOF industrial robots. The main contributions are as follows:

1) Identification of critical components and limit conditions

(1) Critical Components: Joints 2 and 3 carry 99.38% of the static load, making their corresponding upper arm and forearm links the primary targets for lightweight design. Prioritizing weight reduction in these components most effectively reduces joint loads and overall system inertia.

(2) Limit Load Condition: The fully extended arm configuration shown in Fig. 8 constitutes the most severe condition for structural static strength analysis. Compared to the official maximum equivalent load moment of 108 N·m for J_2 and J_3, the simulated moments for J_2 and J_3 reach 154.68 N·m and 27.44 N·m, respectively. Notably, the load on Joint 2 reaches 143% of its rated value, confirming that the identified configuration indeed represents a "hazardous condition" capable of causing structural overload. These torque results serve as crucial input loads for robot limit strength verification and lightweight design, and any optimized topological configuration must satisfy material allowable stress and deformation constraints under this extreme load.

2) Proposal of dimensionality reduction optimization strategy

The torque response and optimization behavior of joints 4-6 demonstrate that wrist joint configurations have negligible influence on global static performance. This finding carries significant practical value: for static performance optimization of such 6-DOF robots, a dimensionality-reduction strategy can be implemented by constraining the hazardous configuration search from the full 6-dimensional joint space to the 2-dimensional subspace spanned solely by Joints 2 and 3. This approach substantially reduces computational expense while enabling rapid structural design iteration.

3) Establishment of performance evaluation benchmark

Finite element analysis of the identified hazardous configuration yields corresponding deformation and stress distributions [38], establishing a benchmark reference for evaluating lightweight design effectiveness. Provided that kinematic parameters remain unchanged, the working conditions and loads characterized in this study can further serve as invariant inputs for assessing the static performance of optimized structural designs.

4) Causes of the torsional phenomenon and result reliability

During the Adams-MATLAB co-simulation, minor torsional deformation was observed in the forearm. This phenomenon primarily stems from modeling and simulation approximations, including potential discrepancies in mass and centroid parameters, slight misalignments in joint coordinate definitions, and cumulative numerical or compliance effects. It should be emphasized that this torsion does not represent actual physical deformation of the robot, but rather arises from inherent modeling simplifications. As evidenced in Table VI, the maximum relative error in joint torques between MATLAB and Adams remains within acceptable limits, with both methodologies consistently identifying the same hazardous configuration and maximum joint torque. Therefore, the observed torsional effect has negligible impact on the substantive conclusions, and all reported torques corresponding to the hazardous posture are derived from the validated model to ensure reliability.

IV. Conclusions

This study addresses the static hazardous configuration identification for the KUKA KR3 R540 industrial robot by successfully establishing an automated analysis framework based on PSO and Adams-MATLAB co-simulation. This framework effectively integrates MATLAB's efficiency in optimization algorithms with Adams' high precision in multi-body dynamics computation, providing a reliable solution for accurately locating hazardous configurations within high-dimensional joint spaces. Through this framework, the research precisely identifies the most hazardous static posture under gravitational field and its corresponding maximum joint loads. The ten independent PSO runs demonstrated excellent robustness, with all executions consistently converging to the same optimal region, exhibiting a standard deviation of merely 0.82 N·m in total torque. Results demonstrate that when the robot adopts the fully extended arm configuration, the combined joint driving torque reaches its peak, with Joints 2 and 3 serving as the primary load-bearing components while wrist joints contribute negligibly. The extreme load conditions and boundary parameters established in this study provide crucial inputs for subsequent structural lightweight design and topological optimization of the upper arm and forearm links. Furthermore, cross-validation of co-simulation results reveals that the maximum joint torque discrepancy between PSO optimization and independent Adams high-fidelity computation remains below 0.0711%, thoroughly verifying the effectiveness and accuracy of both the methodology and conclusions.

While this research provides an effective solution for static hazardous configuration identification in industrial robots, several limitations warrant attention and guide future research directions. First, the multi-rigid-body assumption neglects link and joint flexibility, which may introduce deviations in ultra-high-precision or lightweight design scenarios. Second, the model omits joint friction and actuator dynamics, somewhat simplifying actual joint loading conditions. Finally, the focus on static conditions excludes dynamic torque peaks arising from inertial forces during motion. Future work will develop rigid-flexible coupling dynamic models and, building upon this foundation, pursue dynamic hazardous configuration identification encompassing complete motion trajectories.

Conflict of Interest

The authors declare no conflict of interest.

Author Contributions

LZ conducted the research, performed the data analysis, and drafted the initial manuscript; ADC supervised the overall research direction, guided the entire research process, and provided constructive feedback and revisions to enhance the quality of the manuscript; all authors had approved the final version.

Acknowledgment

The authors wish to thank the editors and the anonymous reviewers for their constructive comments. We also extend our sincere gratitude to Professor Aldrin D. Calderon for his invaluable guidance and support throughout this research.

References

[1] Y. Mi and A. D. Calderon, "Current status and perspectives of research on upper limb rehabilitation robots," in *Proc. 2024 10th Int. Conf. Electr. Eng., Control and Robot. (EECR)*, 2024, pp. 129–133. doi: 10.1109/EECR60807.2024.10607285

[2] L. Zhang, A. D. Calderon, and W. Cui, "Research progress and prospect of industrial robot," in *Proc. Int. Conf. Mech. Eng. Appl. Composite Mater., Singapore: Springer*, 2023, pp. 355–368. doi: 10.1007/978-981-97-1678-4_34

[3] S. Li and A. D. Calderon, "Review of the current research status and constraints of wall-climbing robots," in *Proc. 2023 6th Int. Conf. Robot., Control Autom. Eng. (RCAE)*, 2023, pp. 44–49. doi: 10.1109/RCAE59706.2023.10398765

[4] B. Siciliano and O. Khatib, *Springer Handbook of Robotics*, eds., Cham, Switzerland: Springer, 2016.

[5] A. L. Umbay, A. D. Calderon, E. B. Ang *et al.,* "Development and implementation of a 6-DOF robotic arm with machine vision for sorting application," in *Proc. 2024 3rd Int. Conf. Autom., Robot. Comput. Eng. (ICARCE)*, 2024, pp. 103–106. doi: 10.1109/ICARCE63054.2024.00027

[6] Y. Zhang, A. Müller, and F. Gao, "Dynamic load-carrying capacity of serial robots considering joint torque limits," *Mech. Mach. Theory*, vol. 169, 104625, 2022. doi: 10.1016/j.mechmachtheory.2021.104625

[7] V. Zanotto, A. Gasparetto, A. Lanzutti *et al.,* "Experimental validation of minimum time-jerk algorithms for industrial robots," *J. Intell. Robot. Syst.*, vol. 64, no. 2, pp. 197–219, 2011. doi: 10.1007/s10846-010-9533-5

[8] Z. Wang and M. Schwager, "Kinematic multi-robot manipulation with no communication using force feedback," in *Proc. 2016 IEEE Int. Conf. Robot. Autom. (ICRA*), 2016, pp. 427–432. doi: 10.1109/ICRA.2016.7487163

[9] M. Mohammadnia, N. Kashiri, F. Braghin *et al.,* "Flux regulation for torque-controlled robotics actuators," in *Proc. 2019 19th Int. Conf. Adv. Robot. (ICAR)*, 2019, pp. 93–98. doi: 10.1109/ICAR46387.2019.8981588

[10] L. Liu and A. D. Calderon, "Optimization design of semi-active suspension for vehicles based on LQR optimal control," *J. Phys.: Conf. Ser*., vol. 2785, no. 1, 012005, 2024. doi: 10.1088/1742-6596/2785/1/012005

[11] D. Wang, D. Tan, and L. Liu, "Particle swarm optimization algorithm: An overview," *Soft Comput*., vol. 22, no. 2, pp. 387–408, 2018. doi: 10.1007/s00500-016-2474-6

[12] J. C. Santos, J. M. Sousa, and P. Costa, "Robot trajectory planning using multi-objective optimization," *Robot. Comput. and Comput. Integr. Manuf*., vol. 68, 102076, 2021. doi: 10.1016/j.rcim.2020.102076

[13] J. Huang, "Research on robot arm trajectory optimization based on an improved particle swarm optimization algorithm," *J. Jiujiang Univ. (Nat. Sci. Ed.)*, vol. 39, no. 3, pp. 90–93, 125, 2024. doi: 10.19717/j.cnki.jjun.2024.03.019 (in Chinese)

[14] R. C. Izquierdo, A. R. Cukla, F. J. Lorini *et al.,* "Optimal two-step collision-free trajectory planning for cylindrical robot using particle swarm optimization," *J. Intell. Robot. Syst*., vol. 108, no. 4, 56, 2023. doi: 10.1007/s10846-023-01903-5

[15] H. Hobbani, F. Perez-Peña, and K. Schmidt, "Modelling and identification of a tracked mobile robot: A real-time feasible approach using particle swarm optimization and information criteria," *Int. J. Control Autom. Syst*., vol. 23, no. 8, pp. 2687–2703, 2025. doi: 10.1007/s12555-025-0388-8

[16] A. S. Kumar, S. Naveen, R. Vijayakumar *et al.,* "An intelligent fuzzy-particle swarm optimization supervisory-based control of robot manipulator for industrial welding applications," *Sci. Rep*., vol. 13, no. 1, 8253, 2023. doi: 10.1038/s41598-023-35189-2

[17] M. S. Elhadidy, W. S. Abdalla, A. A. Abdelrahman *et al.,* "Assessing the accuracy and efficiency of kinematic analysis tools for six-DOF industrial manipulators: The KUKA robot case study," *AIMS Math*., vol. 9, no. 6, pp. 13944–13979, 2024. doi: 10.3934/math.2024678

[18] Z. Zhang, A. D. Calderon, X. Huang *et al.,* "Design and driving performance study of soft actuators for hand rehabilitation training," *Med. Devices: Evid. Res*., pp. 237–260, 2024. doi: 10.2147/MDER.S476464

[19] V. Kumar, "Kinematics/dynamics analysis with ADAMS/MATLAB co-simulation of a SolidWorks-designed spatial robot arm with control and validation of results," in *Machines, Mechanism and Robotics: Proc. iNaCoMM 2019*, I. N. Kar, J. S. Ghosh, A. K. Samantaray, and P. M. Pathak, Eds. Singapore: Springer, 2021, pp. 1197–1209. doi: 10.1007/978-981-15-5113-0_103

[20] J. Wu, J. Chen, J. Yang *et al.,* "Dynamic simulation analysis of robots based on ADAMS and MATLAB," *Comput. Simul*., vol. 41, no. 12, pp. 509–516, 2024. (in Chinese)

[21] Y. Xiong, P. Chen, Y. Wang *et al.,* "Leg motion control system of a simulated grasshopper robot based on ADAMS and MATLAB co-simulation," *Mech. Electr. Eng. Technol*., vol. 52, no. 3, pp. 194–198, 2023. (in Chinese)

[22] Y. Huang, Q. Li, and C. Feng, "Dynamic analysis of 6DOF industrial robot based on MATLAB," *Internal Combustion Engine Parts*, no. 14, pp. 70–72, 2024. doi: 10.19475/j.cnki.issn1674-957x.2024.14.010 (in Chinese)

[23] J. Du, W. Zhang, H. Wang *et al.,* "Dynamic analysis and simulation study of upper-limb exoskeleton rehabilitation robot," *Mach. Manuf. Autom*., vol. 54, no. 1, pp. 135–142, 2025. doi: 10.19344/j.cnki.issn1671-5276.2025.01.029 (in Chinese)

[24] N. Wan, "Research on motion planning of six degrees of freedom manipulator," M.S. thesis, School of Mechanical Engineering, Yanshan Univ., Qinhuangdao, China, 2024. doi: 10.27440/d.cnki.gysdu.2024.001416 (in Chinese)

[25] J. Kennedy and R. Eberhart, "Particle swarm optimization," in *Proc. ICNN'95—Int. Conf. Neural Netw*., 1995, vol. 4, pp. 1942–1948. doi: 10.1109/ICNN.1995.488968

[26] F. H. Ajeil, I. K. Ibraheem, M. A. Sahib *et al.,* "Multi-objective path planning of an autonomous mobile robot using hybrid PSO-MFB optimization algorithm," *Appl. Soft Comput*., vol. 89, 106076, 2020. doi: 10.1016/j.asoc.2020.106076

[27] M. Hu, H. Wang, and X. Pan, "Global structural optimization design of collaborative robots based on orthogonal design," *J. Jilin Univ. (Eng. Technol. Ed.)*, vol. 51, no. 1, pp. 370–378, 2021. doi: 10.13229/j.cnki.jdxbgxb20190838 (in Chinese)

[28] Y. Bao, W. Zhao, and M. Zhu, "Dynamic simulation of medium-small group arc-welding robot based on MATLAB and Adams," *Control Eng.*, vol. 30, no. 9, pp. 1585–1591, 2023. doi: 10.14107/j.cnki.kzgc.20210829 (in Chinese)

[29] L. H. Lijun and A. D. Calderon, "Study of the shift process of a hydrodynamic automatic transmission considering the vehicle driveline system," in *Proc. 4th Int. Conf. Mech., Electron., Electr. Autom. Control (METMS)*, vol. 13163, 2024, pp. 1815–1825. doi: 10.1117/12.3030212

[30] H. Wu and A. D. Calderon, "A summary of the development of autonomous vehicle," in *Proc. 2023 6th Int. Conf. Robot., Control Autom. Eng. (RCAE)*, 2023, pp. 174–180. doi: 10.1109/RCAE59706.2023.10398804

[31] H. Gu, X. Hu, and J. Mao, "Joint simulation of kinematics analysis and trajectory planning of 6R robot based on ADAMS and MATLAB," *J. Yancheng Inst. Technol. (Nat. Sci. Ed.)*, vol. 35, no. 4, pp. 62–68, 2022. doi: 10.16018/j.cnki.cn32-1650/n.202204012 (in Chinese)

[32] H. Huang, "Research on lightweight design of industrial manipulators," M.S. thesis, School of Robotics and Advanced Manufacturing, Harbin Inst. Technol., Harbin, China, 2021. doi: 10.27061/d.cnki.ghgdu.2021.001045 (in Chinese)

[33] L. Chen, "Structural design and dynamic analysis of heavy-duty industrial robot driven by large torque," M.S. thesis, School of Mechatronic and Automotive Engineering, Yantai Univ., Yantai, China, 2023. doi: 10.27437/d.cnki.gytdu.2023.000348 (in Chinese)

[34] F. Sun, Y. Chen, Y. Wu *et al.,* "Motion planning and cooperative manipulation for mobile robots with dual arms," *IEEE Trans. Emerg. Topics Comput. Intell.*, vol. 6, no. 6, pp. 1345–1356, 2022. doi: 10.1109/TETCI.2022.3146135

[35] M. Zhang, X. Kong, F. Ma *et al.,* "Optimization of front axle suspension stiffness based on ADAMS–Simulink co-simulation," *Automobile Appl. Technol.*, vol. 50, no. 8, pp. 77–81, 2025. doi: 10.16638/j.cnki.1671-7988.2025.008.015 (in Chinese)

[36] Z. Li, "Simulation analysis of commercial vehicle seat suspension based on ADAMS and Simulink," M.S. thesis, School of Automotive and Traffic Engineering, Liaoning Univ. Technol., Jinzhou, China, 2019. (in Chinese)

[37] P. Corke, W. Jachimczyk, and R. Pillat, *Robotics, Vision & Control: Fundamental Algorithms in MATLAB*, 3rd ed. Cham, Switzerland: Springer, 2023. doi: 10.1007/978-3-031-07262-8

[38] Z. Zhang and A. D. Calderon, "Modeling and analysis of the segmented gas finger rehabilitation training actuator based on ABAQUS," in *Proc. 2023 5th Int. Conf. Robot., Intell. Control Artif. Intell. (RICAI)*, 2023, pp. 39–43. doi: 10.1109/RICAI60863.2023.10489268

Copyright © 2026 by the authors. This is an open access article distributed under the Creative Commons Attribution License which permits unrestricted use, distribution, and reproduction in any medium, provided the original work is properly cited (CC BY 4.0).